J. Fluid Mech. (1980), *vol.* 99, *part* 4, *pp.* 687–703
Printed in Great Britain

Geostrophic fronts, bores, breaking and blocking waves

By MELVIN E. STERN
Graduate School of Oceanography,
University of Rhode Island, Kingston, R.I. 02881

(Received 28 June 1979 and in revised form 17 September 1979)

An undisturbed geostrophic density current flows along a vertical wall (the coast) with the free streamline (the front) located at a distance L from the wall which is comparable to the Rossby radius of deformation. Finite amplitude perturbations with downstream wavelengths much larger than L are discussed, and it is shown that the slope of the front in the horizontal plane increases with time. Some perturbations tend to 'break' seaward by developing large transverse velocities away from the coast. The temporal evolution of some perturbations is such as to completely 'block' the upstream flow, but the subsequent behaviour is beyond the scope of the theory. We also discuss the propagation of the nose of the intrusion when a density current debouches from a coastal source and then flows along the coastal boundary.

1. Introduction

When fresh water from a small coastal source debouches into a large mass of salt water the buoyancy force causes lateral spreading, and the Coriolis force deflects the light water to the coast. Behind the nose of the intrusion (the 'bore') a geostrophic coastal current is established. The rate of propagation of the bore and the dynamics of nonlinear waves on the trailing geostrophic front are the subjects of this paper.

Some of the effects to be discussed in a simplified theoretical model are illustrated and motivated by a qualitative experiment (see figure 1, plate 1) in which relatively light fluid debouches into a rotating channel. The source region (not shown) for the light fluid is in the corner of the rotating (5 s period) rectangular tank (13 cm wide × 100 cm long) and consists of a thin (2 mm) walled vertical cylinder (2 cm diameter) with its open mouth located 0·8 cm below the parabolic free surface of the salt water whose initial mean depth was 11 cm. Dyed fresh water ($0{\cdot}25 \times 10^{-3}$ g cm^{-3} less than the salt water) is fed into the bottom of the cylinder by a vertical capillary tube connected to an overhead feed, the flow rate being 0·96 cm^3 s^{-1}. The cylinder acts as a buffer region, and the light fluid then rises to the free surface and then spreads laterally. In the second of the two experiments shown in figure 1, the external conditions are identical, except that the source region has been modified by placing a thin vertical plate (5 cm long) parallel to the boundary, thereby providing a guiding channel for the water emerging from the top of the cylinder. The 'edge effect' is somewhat different for the two geometrics, but in either case the edge effect is confined to the source region, and the eddy entering on the left-hand side of frame (f) is not an edge effect. The top of the tank in both experiments is sealed by a cellophane cover; but similar waves have been seen in identical experiments with the cover removed and having significant evaporation effects. The noteworthy features of these qualitative experiments are:

0022-1120/80/4512-1730 $02.00

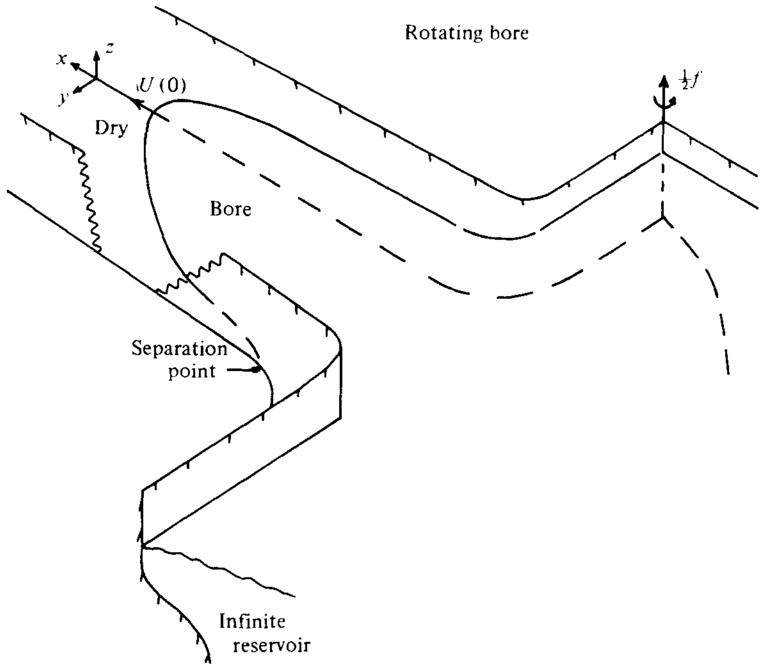

FIGURE 2. Perspective diagram of a realization of a zero absolute vorticity flow in a fluid container rotating with angular velocity $\frac{1}{2}f$. The reservoir is very deep compared to the height of the fluid relative to the level bottom of the channel. The cutaway shows the nose of the bore propagating down the dry channel with speed $U(0)$.

the density current emerging from the source is deflected to the boundary, and a laminar intrusion appears first; perturbations with a horizontal scale larger than the width of the intrusion then appear on the trailing geostrophic front; as these amplify the propagation of the bore is arrested and the upstream flow is diverted normal to the coast and into a geostrophic eddy; the amplitudes of the latter are large compared to the width of the original current; a laminar boundary layer re-forms with a propagating bore, but new eddies are generated downstream – and so on. Most of the time a distinctive tilt of the amplifying wave is seen with a tilt of the crest in the opposite direction to the boundary current; the incipient frontal wave is probably a key element in the mechanism by which the incoming density current is mixed into the interior and by which a mean boundary current is formed. The reader is also referred to Nof (1978) in which a source sink experiment in a two-layer system is discussed, but with no density front.

Since the flow from the source in this experiment is too complex to provide a starting point we will turn to the simpler class of uniform potential vorticity flows (Whitehead, Leetma & Knox 1974), a limiting form of which appears in figure 2. Here we have a very deep and horizontally extensive reservoir, rotating about a vertical axis and containing water which is initially at rest. The barrier (not shown) connecting the reservoir to the long channel is then broken, whereupon water columns flow over the sill and into the channel. These columns conserve their potential vorticity and, since they are forced to decrease their vertical height by a large amount, it follows that the relative vorticity ζ is very nearly balanced by the Coriolis parameter f, i.e. $\zeta = -f$. As the bore propagates down the channel a laminar geostrophic flow is established behind. Therefore the cross-stream height of the free surface must decrease from the right-hand wall to the left-hand wall, and separation from the latter will occur, if the width of the channel exceeds a certain multiple of the Rossby radius of deformation. [The separation effect is especially pronounced if the left-hand wall is slightly curved (Shen 1978)]. After separation the bore and the trailing geostrophic front propagate along the right-hand wall as shown in figure 2. This paper, in contrast to those cited above, concentrates on the dynamics far downstream from the source region. The volume flux far upstream from the nose of the bore is therefore assumed to be known, as well as the corresponding transverse width of the geostrophic current. For a zero absolute vorticity flow these parameters determine the height of the fluid on the wall as well as all the other properties of the upstream flow. In addition to the propagation speed of the nose of the bore, we want to study the properties of nonlinear waves superimposed on the geostrophically balanced flow upstream of the bore. We shall show that these waves exhibit a tendency to 'break', and a tendency to 'block' the upstream flow. Although these effects may be related to the dramatic instabilities which we observed (figure 1) and to the process by which the incoming density current is mixed into the interior, there is no obvious quantitative connexion with the theory because the potential vorticity in the experiment is not zero. Some suggestions for treating the finite potential vorticity front are given in the appendix, and it is hoped that better experiments will be made which will allow a comparison.

The effects discussed herein may be relevant to the lateral mixing which occurs when fresh river water debouches into the ocean, and also when relatively cold water sinks (in wintertime) to the bottom of polar coastal regions (see, for example, Wadhams, Gill & Linden 1979). The abyssal western boundary currents, which are here alluded to, are of great importance in the theory of the thermocline, since these currents determine the mean temperature of the bottom of the ocean. We may also mention the classical meteorological–oceanographic problem of the 'free' front (i.e. no boundaries), and some suggestions for treating this case are also given in the appendix.

2. Long waves with zero absolute vorticity

If η denotes the height of the free surface above the 'level' (geopotential) bottom of a container which rotates about the vertical axis $\mathbf{K}$ with angular velocity $\frac{1}{2}f$, then the hydrostatic equations for the relative horizontal velocity $\mathbf{V}$ can be written as

$$\frac{\partial \mathbf{V}}{\partial t} + (f+\zeta)\,\mathbf{K}\times\mathbf{V} = -\nabla(g\eta + \tfrac{1}{2}\mathbf{V}^2), \tag{2.1a}$$

$$\frac{\partial \eta}{\partial t} + \nabla\,.\,\mathbf{V}\eta = 0, \tag{2.1b}$$

where $\zeta = \mathbf{K}\,.\,\nabla\times\mathbf{V}$ is the relative vorticity. These equations also apply (asymptotically) to a two layer fluid (figure 5*a*) if the acceleration of gravity is reduced by the well-known densimetric factor. These equations imply that $(f+\zeta)/\eta$ is conserved following the motion, and therefore if $f+\zeta = 0$ in the initial state then $f+\zeta = 0$ at all subsequent times t. This first integral may be used, together with the continuity equation (2.1*b*) and one of the two scalar equations in (2.1*a*) to solve the initial-value problem. The three equations are written below in non-dimensional form, using the following scale transformation.

Let $h(x, y, t) = \eta/H$ be the non-dimensional height, where H is the height on the wall ($y = 0$) far upstream ($x = -\infty$) from the nose. The radius of deformation $(gH)^{\frac{1}{2}}f^{-1}$ is taken as the scale for the non-dimensional transverse co-ordinate y, and $L(x, t)$ denotes the corresponding non-dimensional displacement of the front ($h = 0$) from the wall. The following analysis will be restricted to disturbances whose downstream variation is small compared to the cross-stream variation, and thus $\epsilon^{-1}(gH)^{\frac{1}{2}}f^{-1}$ is used as the scale for the non-dimensional x co-ordinate, where $\epsilon \to 0$ in the subsequent asymptotic expansion. Because f is the relative vorticity and $f^{-1}(gH)^{\frac{1}{2}}$ is the y scale, we take $(gH)^{\frac{1}{2}}$ as the scale for the downstream velocity. In order to make the downstream acceleration of the same order as the downstream pressure gradient we take $\epsilon^{-1}f^{-1}$ as the scale for non-dimensional time t. Although the long-wave approximation requires the y component of velocity v to be small compared to u, the relative contributions of (u, v) in the continuity equation must be comparable, and therefore v is scaled by $\epsilon(gH)^{\frac{1}{2}}$. The x-momentum equation, the continuity equation, and the vorticity invariant then assume the non-dimensional forms

$$\frac{\partial u}{\partial t} = -\frac{\partial}{\partial x}(h + \tfrac{1}{2}u^2 + \tfrac{1}{2}\epsilon^2 v^2), \tag{2.2}$$

$$\frac{\partial h}{\partial t} + \frac{\partial uh}{\partial x} + \frac{\partial vh}{\partial y} = 0, \tag{2.3}$$

$$\frac{\partial u}{\partial y} - \epsilon^2 \frac{\partial v}{\partial x} = 1, \tag{2.4}$$

and the boundary conditions are

$$v(x, 0, t) = 0, \quad h(x, L(x, t), t) = 0, \qquad (2.5), (2.6)$$

$$v(x, L, t) = dL/dt, \tag{2.7}$$

$$h(-\infty, 0, t) = 1, \quad v(-\infty, y, t) = 0. \tag{2.8}$$

Equation (2.5) is the wall boundary condition, (2.6)–(2.7) are the free streamline conditions, and (2.8) are the given upstream conditions. These are the classical shallow water (hydrostatic approximation) equations.

A new level of approximation appears when we consider the case in which the downstream variations are small compared to the cross-stream variations, i.e. in the limit when $\epsilon \to 0$ we have

$$\frac{\partial u}{\partial t} = -\frac{\partial}{\partial x}(h + \tfrac{1}{2}u^2), \tag{2.9}$$

$$\frac{\partial h}{\partial t} + \frac{\partial (uh)}{\partial x} + \frac{\partial (vh)}{\partial y} = 0, \tag{2.10}$$

$$\frac{\partial u}{\partial y} = 1, \tag{2.11}$$

together with (2.5)–(2.8).

Note that the asymptotic version of the y component of (2.1 a) gives a geostrophic balance between u and $\partial h/\partial y$, and this balance is implicit in (2.9). To show this we differentiate (2.9) with respect to y, use (2.11) to get $\partial/\partial x(\partial h/\partial y+u) = 0$, and then use (2.8) to obtain the geostrophic equation

$$u = -\partial h/\partial y \tag{2.12}$$

for the downstream velocity.

Equation (2.11) implies that u must be a linear function of y at all (x,t), (2.12) implies that h must be quadratic, and more explicitly we have

$$u(x,y,t) = U(x,t)-(L(x,t)-y) \tag{2.13}$$

$$h(x,y,t) = U(L-y)-\tfrac{1}{2}(L-y)^2 \tag{2.14}$$

where the constant of integration U is the velocity on the free streamline $h(x,L,t) = 0$. Two equations connecting (U,L) are obtained from (2.9)–(2.10) as follows.

The height of the fluid on the wall is

$$h(x,0,t) = (U-\tfrac{1}{2}L)\,L, \tag{2.15}$$

the cross-sectional area is

$$\int_0^L h\,dy = \frac{UL^2}{2}-\frac{L^3}{6}, \tag{2.16}$$

the volume transport is

$$\int_0^L uh\,dy = \frac{L^2}{2}\left(U-\frac{L}{2}\right)^2, \tag{2.17}$$

and the wall velocity is

$$u(x,0,t) = U-L. \tag{2.18a}$$

Since $h(x,L,t) = 0$ the integration of the continuity equation (2.10) gives

$$0 = \int_0^L \left(\frac{\partial h}{\partial t}+\frac{\partial(uh)}{\partial x}\right)dy = \frac{\partial}{\partial t}\int_0^L h\,dy+\frac{\partial}{\partial x}\int_0^L uh\,dy, \tag{2.18b}$$

$$0 = \frac{\partial}{\partial t}\left[\frac{UL^2}{2}-\frac{L^3}{6}\right]+\frac{1}{2}\frac{\partial}{\partial x}\left[LU-\frac{L^2}{2}\right]^2, \tag{2.19}$$

where (2.16)–(2.17) have been used. The second equation connecting (U,L) is obtained by substituting (2.13)–(2.14) in (2.9) to obtain

$$\frac{\partial}{\partial t}(U-L) = -\frac{\partial}{\partial x}\frac{U^2}{2}. \tag{2.20}$$

These new long-wave equations (2.19)–(2.20) are valid as long as the value of v [from (2.10)] is $\ll \epsilon^{-1}$. Even if this is initially satisfied, we anticipate that $v \sim dL/dt$ will become large as time increases (wave steepening), and when this occurs one must return to the more primitive equations (2.2)–(2.4). An important simplification in the frontal dynamics has been achieved, however, in the foregoing separation of the transverse (y) co-ordinate. The resulting equations (2.19)–(2.20) are amenable to solution by the method of characteristics, but first we consider some special solutions.

3. Special solutions

We seek solutions of (2.19)–(2.20) having a time invariant functional relation between $U(x,t)$ and $L(x,t)$; i.e. let

$$U = U(L), \quad \frac{\partial U}{\partial t} = U'(L)\frac{\partial L}{\partial t}, \quad \frac{\partial U}{\partial x} = U'(L)\frac{\partial L}{\partial x}$$

and the more general significance of these will appear in §4. Substitution in (2.20)–(2.19) then yields

$$(U'-1)\frac{\partial L}{\partial t} = -UU'\frac{\partial L}{\partial x}, \tag{3.1a}$$

$$-\left(U-\frac{L}{2}+\frac{LU'}{2}\right)\frac{\partial L}{\partial t} = \left(U-\frac{L}{2}\right)(U-L+LU')\frac{\partial L}{\partial x}. \tag{3.1b}$$

By dividing and simplifying these we get

$$\left.\begin{aligned}(U')^2+2U'\frac{(2U-L)}{L-U}-\frac{2U-L}{L} &= 0,\\ U' = -\frac{2U-L}{L-U}\pm\left[\left(\frac{2U-L}{L-U}\right)^2+\frac{2U-L}{L}\right]^{\frac{1}{2}}&,\end{aligned}\right\} \tag{3.2}$$

or

$$U' = 1-\frac{2U}{L\pm[L(2U-L)]^{\frac{1}{2}}}, \tag{3.3}$$

as may be seen by rationalizing the last term. This differential equation may be reduced to quadratures by substituting

$$U = \psi L, \tag{3.4}$$

(3.3) then becomes

$$\frac{d\psi}{\psi-1+2\psi/[1\pm(2\psi-1)^{\frac{1}{2}}]}+\frac{dL}{L} = 0. \tag{3.5}$$

If U and L satisfy (3.3) at some initial time, then (3.1 a, b) imply that and U, L are independent of time at a point $x = x(t)$ which moves with the (propagation) speed:

$$\frac{dx}{dt} = \frac{UU'}{U'-1} = \frac{U}{1-1/U'}. \tag{3.6}$$

In order to discuss the properties of these special solutions, some typical members of (3.3) [or (3.5)] are sketched in figure 3 along with auxiliary curves. The dashed curve

$$U = 1/L+\tfrac{1}{2}L \tag{3.7}$$

obtained by setting $h = 1$ in (2.15) corresponds to the given upstream state ($x = -\infty$). This curve has been terminated on the line $U = L$ where (2.18) vanishes, the reason being that upstream states having negative velocities ($u(-\infty, 0, t) < 0$) have no present interest for us. But this convention does not preclude negative velocities *downstream* from $x = -\infty$. The line $U = \frac{1}{2}L$ in figure 3 corresponds to vanishing height on the wall (cf. 2.15), and (meaningless) negative heights occur in the region $U < \frac{1}{2}L$.

Consider the solution of (3.3) [or (3.5)] with the positive sign, the corresponding curves (figure 3) for which are designated by the $\oplus$ symbol. These solutions have $U' = 0$ at $U = \frac{1}{2}L$; and $U' \to -\infty$ at $L \to 0$ and U finite. Moreover, the function on the right-hand side of (3.3) has a zero at $U/L = 1$, and it is positive for $U < L$. Therefore $U' = 0$ at both $U = \frac{1}{2}L$ and $U = L$, with $0 < U' < 1$ for $U < L$. We see that (3.6) is negative for $U < L$, implying that the local propagation velocity is upstream; whereas downstream propagation occurs for $U > L$.

Consider next the solutions of (3.3) with the negative sign, or

$$U' = 1-\frac{2U}{L-[L(2U-L)]^{\frac{1}{2}}} = 1+\frac{2\psi}{(2\psi-1)^{\frac{1}{2}}-1} \tag{3.8}$$

$$L\frac{d\psi}{dL} = 1-\psi+\frac{2\psi}{(2\psi-1)^{\frac{1}{2}}-1} \tag{3.9}$$

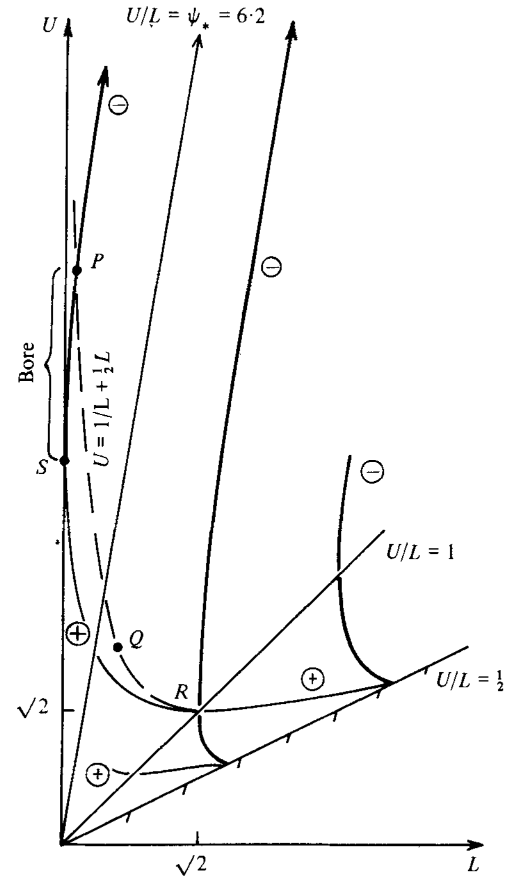

FIGURE 3. The curved heavy lines are some typical solutions for the two (±) families of (3.3). These were constructed by drawing lines of constant slope (3.3) in figure 3 on lines of constant U/L. Points like P, Q, R on the dashed curve represent allowed upstream states. The curve PS represents a 'bore' connected to the upstream state P. The curve RS represents a wedge connected to the upstream state R. Upstream state points like Q, which lie below the line $U/L = 6.2$, can only be connected to wedges and not to bores. Points on the line $U/L = \frac{1}{2}$ correspond to local regions of the density current for which the thickness of the fluid on the wall vanishes. The two sets (±) of curves are, moreover, the Riemann invariants from which the solution of any initial value problem may be constructed, as illustrated in figure 4.

these being designated by the symbol ⊖ in figure 3. The right-hand side of (3.9) has one and only one zero, i.e.

$$1-\psi+\frac{2\psi}{(2\psi-1)^{\frac{1}{2}}-1} \quad \begin{cases} <0 & \text{for} \quad \infty > \psi > \psi_*, \\ >0 & \text{for} \quad \psi_* > \psi > 1, \end{cases} \tag{3.10}$$

$$\psi_* = 6{\cdot}2. \tag{3.11}$$

Therefore the solution of (3.8)–(3.9) which passes through a point (U, L) which lies above the line $U = \psi_* L$ must lie above that line for all L. Likewise the solution passing through a point lying below $U = \psi_* L$ must lie below that line for all L, and must never intersect the U axis. The latter curves have $U' = \infty$ at $U = L$, are double valued, and have $U' = 0$ at $U = \frac{1}{2}L$. The former curves (those lying above $U = \psi_* L$)

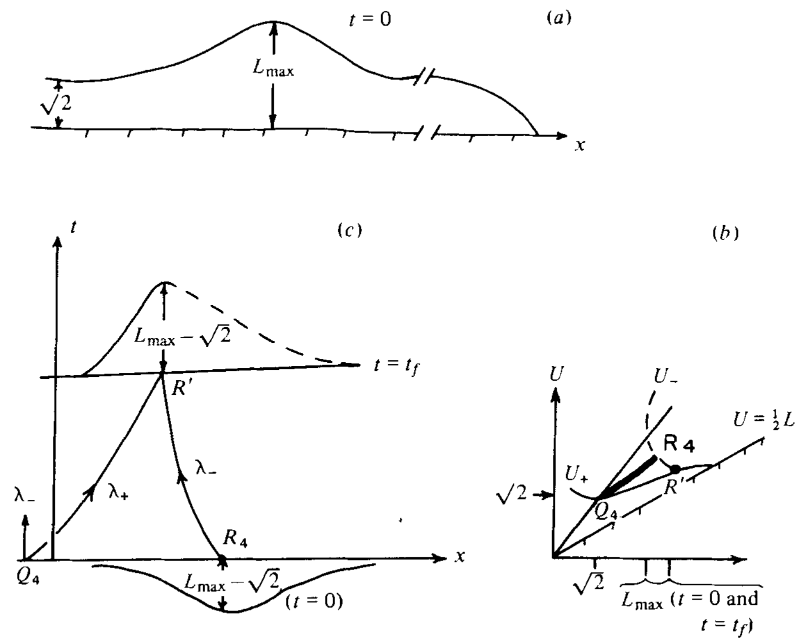

FIGURE 4. Evolution of a blocking wave. (*a*) Initial displacement of the front at some distance behind the bore. (*b*) The curve Q_4R_4 gives the initial distribution of U, and this curve then evolves towards Q_4R' as time increases. (*c*) Evolution in physical space (x, t) of the initial disturbance. λ_- is a characteristic passing through point R_4 and λ_+ is the steeper characteristic passing through Q_4.

have $U' \rightarrow (2U/L)^{\frac{1}{2}} \rightarrow +\infty$ for small L and finite U. As L increases from zero, U increases and the propagation speed (3.6) increases. The propagation speed for curves lying below $U = \psi_* L$ is also positive since (3.8) is negative for $U < L$, and since (3.8) exceeds unity for $U > L$. The dynamical interpretation of these properties of the solution curves follows.

4. Discussion of special solutions

The different branches and parts of the foregoing solution curves correspond to different effects, and the solution corresponding to an intrusion (like figure 5*a*) of a density current is discussed first.

(*a*) *Bores and wedges*

An intrusion must have $L = 0$ at its leading edge, and the corresponding $U(L)$ curve in figure 3 must intersect the U axis. Far upstream from the nose ($L = 0$) we are given the uniform value of L (and U), as represented by some given point like P (figure 3), on the dashed line curve. Through this point pass two solution curves which intersect the U axis. The $\ominus$ solution (the curve PS) was shown to have a local propagation speed which decreases with L, and the nose of this 'bore' therefore advances slower than the rear. An observer moving with the nose sees the front steepen with time, and also a *convergence* of the energy flux. There is also a $\oplus$ solution (not drawn) passing through P and intersecting the U axis, but the propagation velocity for this 'wedge' intrusion increases towards the nose. An observer moving with the nose sees the wedge get thinner with time, and there is a *divergent* energy flux.

A wedge intrusion should not be realizable over 'long' time intervals because frictional forces (not included in the present theory) will eventually become dominant at the leading edge, and slow it down. The 'bore', on the other hand, might evolve into a qualitatively similar realization even though it steepens with time. The neglected $[O(\epsilon^2)]$ inertial terms then become quantitatively important, the nose of the intrusion must be modified, and a bore of 'permanent' shape may evolve. Although the precise nature of the structure of the nose after long time intervals cannot be determined at this stage, the distinction between 'bores' and 'wedges' seems to be sound.

For upstream state points like Q (figure 3) which lie below the line $U/L = \psi_* = 6{\cdot}2$, we have shown that the $\ominus$ solutions do not intersect the axis, and therefore bore solutions do not exist for upstream states satisfying $U \leqslant \psi_* L$. From this and (3.7) it follows that

$$L = \frac{1}{(\psi_* - \frac{1}{2})^{\frac{1}{2}}} = \frac{1}{\sqrt{5{\cdot}7}} \tag{4.1}$$

is the maximum upstream width which will allow a bore to propagate. Wider boundary currents must somehow 'adjust' so that only a small portion (4.1) propagates down the coast, and the nature of this adjustment remains to be elucidated.

The propagation speed of the nose of the bore can be computed as follows. Since $U'(0) = \infty$, eq. (3.6) shows that the nose advances at a speed $U(0)$. The latter is computed by integrating (3.9) from P, where $L = L_p$ is given and $U = 1/L_p + \frac{1}{2}L_p$, to the point $L = 0$. The expression for the nose speed so obtained is as follows:

$$\frac{d\psi}{1-\psi+2\psi/[(2\psi-1)^{\frac{1}{2}}-1]} = d\ln L = d\ln U - \frac{d\psi}{\psi},$$

$$\ln\frac{U(0)}{1/L_p + L_p/2} = -\int_{1/L_p^2+\frac{1}{2}}^{\infty} d\psi\, \frac{1+2\psi/[(2\psi-1)^{\frac{1}{2}}-1]}{\psi[\psi-1-2\psi/[(2\psi-1)^{\frac{1}{2}}-1]]}. \tag{4.2}$$

The latter integral converges when L_p is less than (4.1), and becomes infinite for $L_p = 1/\sqrt{5{\cdot}7}$. In this limit $U(0) = 0$, and the nose of the bore remains stationary until it is 'over-run' by the trailing part of the front, at which point the foregoing asymptotic theory fails.

(*b*) *The quasi-geostrophic breaking wave*

Let us temporarily ignore the above mentioned problem of the long time behaviour of the nose, and turn our attention to the propagation of waves on an otherwise undisturbed front which lies parallel to the coast in the interval $-\infty < x < +\infty$. If the basic geostrophic current is unidirectional then the largest possible width will correspond to the point $R(L = \sqrt{2} = U)$ in figure 3. Suppose that this basic state is perturbed with the initial value $(t = 0)$ of $L(x, t)$ being $L(x, 0) \geqslant \sqrt{2}$, and with $U(x, 0)$ lying along the 'special' $\oplus$ curve passing through R. The propagation speed for such a wave is negative [because $U(L)$ lies below the $U = L$ line], and increases in magnitude as $(L-\sqrt{2})$ increases. Therefore the crest of the front $(\max L)$ moves upstream with the greatest speed, and *the front steepens on the upstream side* of the wave. The transverse velocity dL/dt on the free streamline may be computed with the help of

(3.1 a), and thus we see that

$$v(x, L, t) = \frac{\partial L}{\partial t} + U\frac{\partial L}{\partial x} = \frac{U}{1-U'}\frac{\partial L}{\partial x} \tag{4.3}$$

approaches *plus* infinity as the wave steepens. Note that the large velocities developed during the steepening phase are directed *away* from the *rigid* boundary, and contrast this with the non-rotating problem (Stoker 1957) where the gravity wave develops large velocities towards the rigid boundary. Thus the kinematical constraint on the breaking of large scale horizontal wave is less severe than the corresponding constraint in the classical wave breaking problem. When the x derivative of (2.14) is evaluated at $y = L$ we get $(\partial h/\partial x)_L = U\,\partial L/\partial x$, and therefore (4.3) may be written as

$$v(x, L, t) = \frac{1}{1-U'}\left(\frac{\partial h}{\partial x}\right)_{y=L}. \tag{4.6}$$

Figure 3 shows that $U' = 0$ at point R, and therefore $v \cong \partial h/\partial x$ for small amplitude: $|L-\sqrt{2}| \ll 1$. In this limit the wave in question is quasi-geostrophic with respect to the transverse velocity, as well as with respect to the longitudinal component (2.12).

(c) *Blocking waves*

Let the initial amplitude of the wave discussed above be increased so that (max U, max L) lies on the line $U = \frac{1}{2}L$ in figure 3. Here we have a perturbation with such large negative wall velocities that the height of the fluid on the wall is *initially* zero, and the net transport (2.17) at the section in question ($L = \max L$) is also zero. The propagation speeds (3.6) at this section also vanish, and therefore the net transport is zero at all subsequent times! Thus the current is permanently 'blocked' at max L, while the upstream half of the wave still propagates upstream and steepens as in example (b). We shall subsequently see how such blocking waves can arise from smaller finite amplitude disturbances of a 'non-special' kind.

(d) *Other waves*

Consider once again a basic state with $L = \sqrt{2} = U$ (point R), and now introduce a perturbation in which (U, L) lie along a $\ominus$ curve in figure 3. Since $U' = \infty$ at R there are two possibilities. Either $U-\sqrt{2} > 0$ with $L-\sqrt{2} > 0$, or else $U-\sqrt{2} < 0$ with $L-\sqrt{2} > 0$. In either case we have shown that the propagation velocity is positive, but in the first case (3.6) increases with L whereas the opposite is true when $U-\sqrt{2} < 0$. Therefore the wave steepens on the downstream side in the first case, and steepens on the upstream side in the second case. These waves are related to the classical Kelvin wave in a semi-infinite fluid of uniform depth† because in the limit of $|U-\sqrt{2}| \ll 1$ the transverse velocities vanish. But for finite amplitude the transverse velocities increase in time, and there will be a great difference in the nature of the 'breaking' of the two types of waves. The second case breaks seaward whereas the first case breaks towards the rigid coast.

Although the nature of the breaking and blocking process in all of these cases is beyond the scope of the long wave theory [(2.19)–(2.20)], and the more primitive

† Bennet (1973) (see also Smith 1972) has investigated finite amplitude Kelvin waves in a semi-infinite fluid (no 'front') of uniform potential vorticity, and has shown the tendency of these waves to steepen.

equations (2.2)–(2.4) must be investigated, it would seem almost certain that the evolution of such waves will have important effects on the entire density current, and its lateral mixing with the resting fluid on the seaward side.

5. The initial-value problem

Equations (2.19)–(2.20) may be solved by the method of characteristics. When (2.20) or

$$\frac{\partial U}{\partial t}+U\frac{\partial U}{\partial x}-\frac{\partial L}{\partial t}=0 \tag{5.1}$$

is used to simplify (2.19), the latter may be written as

$$\frac{L}{2}(U-L)\frac{\partial U}{\partial x}+U\frac{\partial L}{\partial t}+(U-L)\left(U-\frac{L}{2}\right)\frac{\partial L}{\partial x}=0. \tag{5.2}$$

When this is added to the product of (5.1) with a multiplier $\alpha(U,L)$ we obtain

$$\alpha\left(\frac{\partial U}{\partial t}+\lambda\frac{\partial U}{\partial x}\right)+(U-\alpha)\left(\frac{\partial L}{\partial t}+\lambda\frac{\partial L}{\partial x}\right)=0 \tag{5.3}$$

where α and $\lambda(U,L)$ are such that

$$\lambda=\frac{\alpha U+\frac{1}{2}L(U-L)}{\alpha}=\frac{(U-L)(U-\frac{1}{2}L)}{U-\alpha} \tag{5.4}$$

The latter part of (5.4) gives a quadratic equation for α, whose two roots are

$$2\alpha_{\pm}=L\pm[L(2U-L)]^{\frac{1}{2}}; \tag{5.5}$$

the corresponding values of λ are

$$\lambda_{\pm}=\frac{U-L}{1\mp[L/(2U-L)]^{\frac{1}{2}}}. \tag{5.6a}$$

We note that both of these λ values are positive if $U>L$, but

$$\lambda_{+}=\frac{U-L}{1-[L/(2U-L)]^{\frac{1}{2}}}>0,\quad \lambda_{-}=\frac{U-L}{1+[L/(2U-L)]^{\frac{1}{2}}}<0,\quad \text{if}\quad L>U. \tag{5.6b}$$

At a point $x=x(t)$ moving with speed $dx/dt=\lambda$, the rate of change of $U(x,t)$, $L(x,t)$ are $dU/dt=\partial U/\partial t+\lambda\partial U/\partial x$ and $dL/dt=\partial L/\partial t+\lambda\partial L/\partial x$. Using these in (5.3) gives $\alpha dU/dt+(U-\alpha)dL/dt=0$ at a point moving with one of the characteristic speeds (5.6a). At such a point the functional relationship $U=U(L)$ obtained by solving the differential equation

$$\alpha(U,L)\,dU+(U-\alpha)\,dL=0$$

is time invariant. When (5.5) is used the differential equation for this Riemann invariant is

$$\frac{dU}{dL}=1-\frac{2U}{L\pm[L(2U-L)]^{\frac{1}{2}}}$$

which is identical to (3.3), i.e. the curves in figure 3 correspond to the Riemann invariants of the initial value problem. We shall now use the method of characteristics to show how the special waves in §§4(b) and 4(c) evolve from a more general class of initial perturbations.

Consider an initial value problem (figure 4) in which $L=\sqrt{2}=U$ at $x=-\infty$, in which L increases downstream to its maximum value $L_{\max}$, and in which U also increases but less rapidly than L. Thus $U < L$ and (5.6*b*) shows that the characteristics have opposing slopes. At the point Q_4 in the upstream region (figure 4) of the perturbation draw a λ_+ characteristic starting from $t = 0$. At all later times the value of U, L on any such curve must lie on the U_+ invariant (figure 4*b*) which passes through the point Q_4: $(\sqrt{2}, \sqrt{2})$. Next consider a λ_- characteristic drawn (figure 4*c*) through the point R_4 having the maximum initial amplitude. This has negative slope and will intersect the previously mentioned λ_+ characteristic as shown in figure 4(*c*). The Riemann invariant for the λ_- curve is constructed by drawing a U_- curve through the known point R_4 in figure 4(*b*). At the time when the λ_+ and λ_- characteristics intersect (at the point labelled R' in figure 4*c*) the corresponding values of (U, L) must satisfy both the previously mentioned Riemann invariants. Consequently R' must be located at the intersection of the U_- characteristic passing through R_4 and the U_+ characteristics passing through Q_4 in figure 4(*b*). Thus we see that the initial state represented by the curve $Q_4 R_4$ in figure 4(*b*) evolves into $Q_4 R'$, the latter being the special wave discussed in §4. After the $Q_4 R'$ phase is reached the wave merely steepens on its upstream side while conserving $L_{\max}$, but the qualitative discussion given above shows that the final value of $L_{\max}$ can exceed its initial value. If the initial $L_{\max}$ in figure 4(*b*) is increased, then the final point R' will lie on the $U = \frac{1}{2}L$ where $h(x, 0, t) = 0$ and blocking (§4*c*) occurs. We conclude that total blocking can evolve from smaller perturbations. This effect as well as the seaward-breaking wave (§4*b*, *d*) may, depending on the role of the short waves, lead to a pronounced 'instability' of the boundary current – such as those in figure 1.

6. Conclusions

Figure 5(*a*) is a schematic diagram of a relatively light liquid flowing from a surface source into a deep and stationary fluid. Our results will be summarized in this context, rather than for the formally equivalent bottom current, because in a laboratory realization of the latter consideration must be given to the deviation of the bottom surface from a geopotential as well as to the Ekman friction.

A bore will propagate along the wall with speed (4.2) provided the upstream width L_p is less than a certain fraction of the radius of deformation (4.1). This result pertains to the case of zero potential vorticity, and the effect of finite potential vorticity may be computed from the generalized theory outlined in the appendix.

An arbitrary long wave bulge (figure 5*b*) behind the nose of the front evolves in time according to equations (2.19)–(2.20). The particular case shown in figure 5(*c*) corresponds to the wave discussed in §5 (see also §4*b*), with the 'wiggly' arrow indicating the amplification and upstream propagation of the front. Whereas this wave is stationary and geostrophic for infinitesimal amplitude, there is upstream propagation for finite amplitude. The seaward component of velocity thereby increases with time until its dimensional value becomes comparable to the downstream velocity, at which stage the long wave theory fails and equations (2.2)–(2.4) must be used. The backward-breaking wave (figure 5*d*) and the forward breaking wave (figure 5*e*) are the Kelvin-like waves discussed in §4. We expect that the modification of the mean flow will be significantly different for waves which break towards the rigid boundary and for those that break seaward.

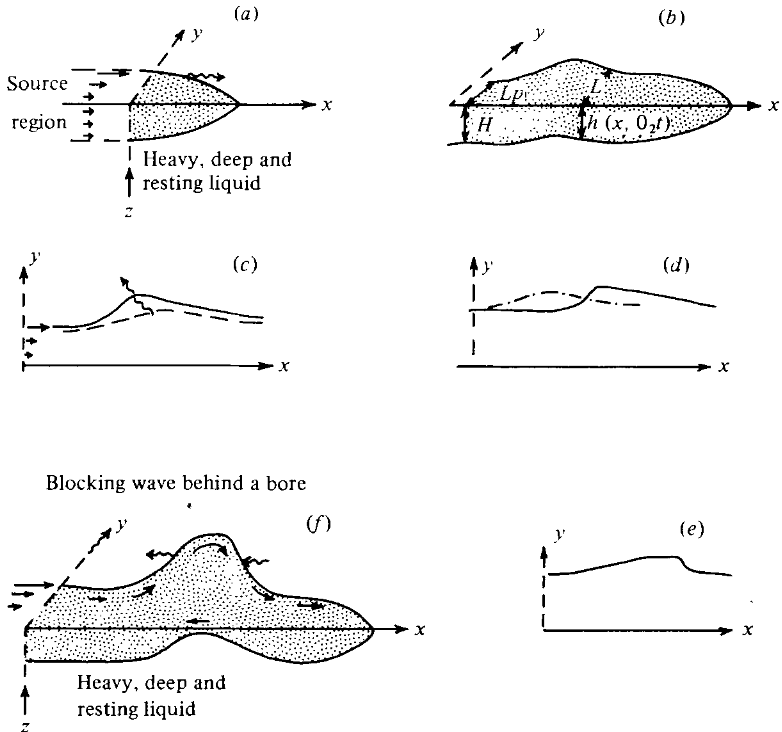

FIGURE 5. (*a*) Surface density current emerging from a source. Straight arrows represent currents, and 'wiggly' arrows are frontal propagation velocities. (*b*) Propagating bore with perturbation in the rear. (*c*) Evolution of a backward-propagating wave. (*d*) Forward-propagating wave with steepening in the rear. (*e*) Forward-propagating wave with forward steepening. (*f*) Blocking wave with stationary crest and upstream propagation.

The blocking wave (figure 5*f*) is a limiting case of (*c*) which occurs when the initial wave amplitude is sufficiently large (§ 5). The amplitude then increases in time until the thickness on the wall vanishes at some cross-section. The total transport through this section vanishes at this, and all subsequent time. The upstream front then propagates upstream as the flow piles up (blocking). The downstream portion of the front also propagates upstream, and this accounts for the mass flow further downstream. But the downstream mass budget is clearly approaching a trauma, and a far reaching modification ('instability') of the entire boundary current, including the bore, is strongly suggested. Perhaps the propagation of the bore will be arrested, as the boundary current in the blocked region is diverted normal to the coast and a large eddy is formed. At a later stage the eddy might detach, allowing the boundary current and the nose of the front to re-form. A new bore could then propagate along the wall until a sufficiently large perturbation causes the whole process to recur, thereby giving rise to a (geostrophic) turbulent coastal current which mixes laterally into the adjacent sea by means of the eruptions and eddies mentioned above. Although this is a highly speculative picture of the post steepening phase, something like this appears to occur in our laboratory experiment (figure 1).

Appendix. Remarks and suggestions

(*a*) *Short wave dispersion.* The question arises as to whether the steepening of the long waves (§ 4) can be compensated by the dispersion of the short waves which are generated. To investigate this one must return to the more primitive equations [(2.2)–(2.4)] and solve these with ϵ finite, but this nonlinear problem is difficult because the y co-ordinate can no longer be separated. Some insight into the dispersion may be obtained, however, by considering the behaviour of short *infinitesimal* amplitude waves on an undisturbed front which is parallel to the coast in the interval

$$-\infty < x < +\infty.$$

Let $\overline{u}(y)$ be the undisturbed linear current; let $\overline{h}(y)$ be the corresponding undisturbed height; let $(u', v', h') \exp i(x-ct)$ be the perturbations, where c is the non-dimensional phase speed for non-dimensional wave number unity (the parameter ϵ carries the dimensional value of the wavenumber). The *linearization* of the 'primitive' equations (2.2)–(2.4) then gives

$$(\overline{u}-c)\,u' = -h',$$

$$(\overline{u}-c)\,h' + \overline{h}u' - i\,\frac{d}{dy}\,(v'\overline{h}) = 0,$$

$$\frac{du'}{dy} - \epsilon^2 iv' = 0;$$

the result of eliminating (v', h') is

$$\frac{d}{dy}\,\overline{h}\,\frac{du'}{dy} - \epsilon^2 u'[\overline{h} - (\overline{u}-c)^2] = 0. \tag{A 1}$$

The boundary condition $v' = 0$ at $y = 0$ implies

$$\frac{du'(0)}{dy} = 0 \tag{A 2}$$

and we require finite $du'(L)/dy$ in order that v' be finite on the free streamline ($\overline{h} = 0$). When these two boundary conditions are used in the integration of (A 1) we obtain

$$\int_0^L dy[\overline{h} - (\overline{u}-c)^2]\,u' = 0. \tag{A 3}$$

A power series expansion in ϵ^2,

$$c = c_0 + c_2\epsilon^2 + c_4\epsilon^4 + \dots, \quad u' = u_0'(y) + \epsilon^2 u_2'(y) + \dots,$$

may be used to solve the eigenfunction problem, and substitution in (A 1) gives $du_0'/dy = 0$ for the leading term. The leading term in (A 3) is then

$$u_0' \int_0^L dy[\overline{h} - (\overline{u} - c_0)^2] = 0 \tag{A 4}$$

which is a quadratic equation for c_0 with coefficients that depend on the basic flow. These non-dispersive long waves are merely the small-amplitude solutions of (2.19)–(2.20). The next term c_2 in the above expansion gives the first-order effect of dispersion. Perhaps a theory can be devised which incorporates this effect with the nonlinear effects in (2.19)–(2.20).

(*b*) *Topographic effects on density currents.* The question arises as to whether our long-wave theory can be generalized for the case of a current flowing along a bottom which slopes in the direction normal to the coast. If η represents the local height of the fluid layer above the sloping bottom then a term $[-g\nabla$ (bottom elevation)] must be added to the right-hand side of (2.1*a*). This y directed force requires no alteration in the asymptotic equations (2.9)–(2.11), but (2.12) is modified to

$$u = -\frac{\partial h}{\partial y} - \frac{\partial M}{\partial y} \tag{A 5}$$

where M is the non-dimensional topographic height. Equation (2.14) must then be modified by adding a term $M(y) - M(L)$ to the left-hand side. If (2.11) and (A 5) are satisfied then the expression

$$\frac{\partial u}{\partial t} + \frac{\partial}{\partial x}\left(h + \frac{u^2}{2}\right) \tag{A 6}$$

will clearly have a vanishing y derivative. Therefore if (A 6) vanishes at any y, say $y = L(x,t)$, then (2.9) will be satisfied at *all* y. But substituting (2.13) and the modified (2.14) into (A 6), by evaluating it at $y = L$ and by setting the result equal to zero we obtain one equation for L, U (involving $M(L)$). The integrated continuity equation (2.18*a*) provides the second relation, and thus we obtain the generalization of (2.19)–(2.20) for the case of a cross-stream topographic variation. Both systems are autonomous second order equations, and there will be (almost certainly) wave breaking in this topographic problem. The quantitative results (e.g. the bore speed) will, however, be different.

A qualitative change in the aforementioned structure of the nonlinear equation for long waves occurs, however, if there is a *downstream* variation $M(x)$ (using the appropriate scaling in non-dimensionalizing) in the bottom elevation. Although equations (2.12), (2.11), (2.10) are unaltered, where h is again the height of the free surface above the bottom, the term $-M'(x)$ must be added to the right-hand side of (2.9). This term must also be added to the right-hand side of (2.20), but (2.19) is unaltered. Thus we now have an *inhomogeneous* differential equation for $L(x,t), U$. Such an inhomogenous force $-M'(x)$ will occur when a bottom density current flows radially on a *plane* which is perpendicular to the axis of rotation, and which is therefore inclined at a slope relative to the parabolic level surfaces. Such a bottom surface simulates the planetary 'β-effect' on a sphere.

(*c*) *Finite potential vorticity*. The key step in the simplification of the frontal problem is the separation of the y variable, and the question arises as to whether a similar reduction of the field problem can be achieved for less specialized flows. With no restriction placed on the potential vorticity, and with the same scaling for u, v, h etc. as was used in § 2, we obtain the following *long wave* ($\epsilon \to 0$) momentum and continuity equations:

$$\frac{\partial u}{\partial t} - \left(1 - \frac{\partial u}{\partial y}\right) v + \frac{\partial}{\partial x}\left(h + \frac{u^2}{2}\right) = 0, \tag{A 7}$$

$$u = -\frac{\partial h}{\partial y}, \tag{A 8}$$

$$\frac{\partial h}{\partial t} + \frac{\partial hu}{\partial x} + \frac{\partial hv}{\partial y} = 0, \tag{A 9}$$

these being the generalization of (2.9)–(2.11). The y derivative of (A 7) yields

$$0 = \frac{\partial}{\partial t}(-u_y) + \frac{\partial}{\partial y}[(1-u_y)v] + \frac{\partial}{\partial x}[u(1-u_y)] = \frac{d}{dt}(1-u_y) - (1-u_y)\frac{1}{h}\frac{dh}{dt},$$

or

$$\frac{d}{dt}\left(\frac{1-u_y}{h}\right) = 0 \tag{A 10}$$

which is the asymptotic version of the law of conservation of potential vorticity. Conversely, if (A 10) is satisfied along with (A 9) and (A 8), then the y derivative of the left-hand side of (A 7) will vanish. Therefore equation (A 7) will hold at *all* y provided

$$\frac{\partial u}{\partial t}-\left(1-\frac{\partial u}{\partial y}\right)v+\frac{\partial}{\partial x}\left(h+\frac{u^2}{2}\right)=0 \quad \text{at } one \text{ value of } y. \tag{A 11}$$

For a current with uniform potential vorticity, $1/\mathscr{H}$, or

$$\frac{1+h_{yy}}{h}=\frac{1}{\mathscr{H}}, \tag{A 12}$$

equations (A 10) (and (A 8)) are satisfied at all time. Therefore it only remains to choose the constants of integration of (A 12) such that (A 11) is satisfied along with the continuity equation. If there is a free streamline $h(x,L(x,t),t)=0$ at a distance L from a vertical wall ($y=0$), then we write the solution of (A 12) as

$$\begin{aligned} h(x,y,t) &= \mathscr{H}\left[1-\cosh\frac{L-y}{\mathscr{H}^{\frac{1}{2}}}\right]+\mathscr{H}^{\frac{1}{2}}U(x,t)\sinh\frac{L-y}{\mathscr{H}^{\frac{1}{2}}}, \\ u(x,y,t) &= -\mathscr{H}^{\frac{1}{2}}\sinh\frac{L-y}{\mathscr{H}^{\frac{1}{2}}}+U\cosh\frac{L-y}{\mathscr{H}^{\frac{1}{2}}}. \end{aligned} \tag{A 13}$$

We now use these to evaluate (A 11) at $y=L$, at which point $[1-u_y]_{h=0}=0$ and the term containing v in (A 11) vanishes. The result is identical to (2.20). The second equation connecting (U,L) comes from substituting (A 13) in the integrated continuity equation (2.18*b*), and this generalization of the differential equation will have hyperbolic functions of L as coefficients. Although the solutions of this system have not been investigated, it is quite likely that such qualitative effects as bores, breaking, and blocking will also appear for this *finite* potential vorticity boundary current.

The important problem of a *free* (no walls) frontal wave can be studied by using models in which the potential vorticity is piecewise uniform. Consider, for example, two semi-infinite fluids of the same density, separated by a vertical discontinuity surface at $y=L(x,t)$. The thicker fluid in the region $L>y>-\infty$ has a non-dimensional potential vorticity equal to unity, and the fluid in $L<y<\infty$ has the uniform potential vorticity $1/\mathscr{H}>1$. The corresponding solutions of (A 12) which are continuous at $y=L$ and which have $u(x,\pm\infty,t)=0$ are

$$h(x,y,t)=\begin{cases}\mathscr{H}+A(x,t)\exp-(y-L)\mathscr{H}^{-\frac{1}{2}}, & y>L\\ 1+(\mathscr{H}-1+A)\exp(y-L), & y<L.\end{cases} \tag{A 14}$$

We also require $v(x,\pm\infty,t)=0$, and consequently (A 11) is automatically satisfied. The two equations for determining $L(x,t)$, $A(x,t)$ then come from the continuity equation and the kinematical conditions: $v(L^{\pm})=\partial L/\partial t+u(x,L^{\pm},t)\,\partial L/\partial x$ on either side ($L^{\pm}$) of the discontinuity surface. These equations are obtained by substituting (A 14) and (A 8) in

$$\frac{\partial}{\partial t}\int_{L^{\pm}}^{\pm\infty}h\,dy+\frac{\partial}{\partial x}\int_{L^{\pm}}^{\pm\infty}uh\,dy=0. \tag{A 15), (A 16}$$

The undisturbed state ($\partial L/\partial x=0$) of this model may be viewed as the limit of an equilibrium geostrophic shear flow in which the potential vorticity increases *monotonically* from 1 to $1/\mathscr{H}$. This equilibrium is probably stable to small perturbations, according to the quasi-geostrophic Rayleigh inflexion theorem (Stern 1975, p. 69), and therefore (A 15), (A 16) are probably hyperbolic. The mathematical and physical properties will change most significantly, however, if we have a third region with a uniform potential vorticity $1/H_*$ lying between the other two regions. There will be an extremum of undisturbed potential vorticity if $1/H_*$ either exceeds $1/\mathscr{H}$ or is less than unity; and consequently there will probably be an energy source for amplifying infinitesimal perturbations. The waves in such a system may therefore be expected to exhibit 'stronger' effects on the current than occurs in the zero absolute vorticity model. Studies of the variable potential vorticity model might be directed towards waves observed on the Gulf Stream front, and perhaps the dramatic phenomenon of ring formation (Fuglister & Worthington 1951) might be interpretable as an unstable blocking wave.

REFERENCES

Bennett, J. R. 1973 A theory of large amplitude Kelvin waves. *J. Phys. Oceanog.* **3**, 57–60.

Fuglister, F. C. 1972 Cyclonic rings formed by the Gulf Stream. In *Studies in Physical Oceanography I*, pp. 137–167. Gordon and Breach.

Fuglister, F. C. & Worthington, L. V. 1951 Some results of a multiple ship survey of the Gulf Stream. *Tellus* **3**, 1–14.

Nof, D. 1978 On geostrophic adjustment in Sea Straits and wide Estuaries. *J. Phys. Oceanog.* **8**, 867–872.

Shen, C. Y. 1978 The rotating hydraulics of steady flow in open channels. Dissertation, University of Rhode Island.

Smith, R. 1972 Nonlinear Kelvin and coastal shelf waves. *J. Fluid Mech.* **52**, 379–391.

Stern, M. E. 1975 *Ocean Circulation Physics*. Academic.

Stoker, J. J. 1957 *Water Waves*. Wiley-Interscience.

Wadhams, P., Gill, A. E. & Linden, P. F. 1979 Transects by Submarine of the East Greenland Polar Front. Submitted to D.S.R.

Whitehead, J. A., Leetmaa, A. & Knox, R. A. 1974 Rotating hydraulics of strait and sill flows. *J. Geophys. Fluid Dyn.* **6**, 101–125.

Figure 1. Dyed fresh water emerging from a small circular source located (but not seen) in the lower left-hand corner of the rotating rectangular tank, the top of which is covered (see text). Experiment 1: (*a*) nose of intrusion is 20 cm downstream from source and time after starting is 1 min 19 s; (*b*) after 2 min, amplifying wave behind nose is seen; (*c*) after 9 min 16 s, showing evolved eruptions of the coastal jet together with smaller incipient waves. Experiment 2: (*d*) after 2 min 26 s with identical conditions except for source geometry (see text); (*e*) after 3 min 56 s, note that the large-amplitude wave is forming a detached vortex; (*f*) after 6 min 29 s, a big eddy has propagated downstream in the left-hand side of the picture and a new cusped wave is seen forming on the laminar coastal current in this region.

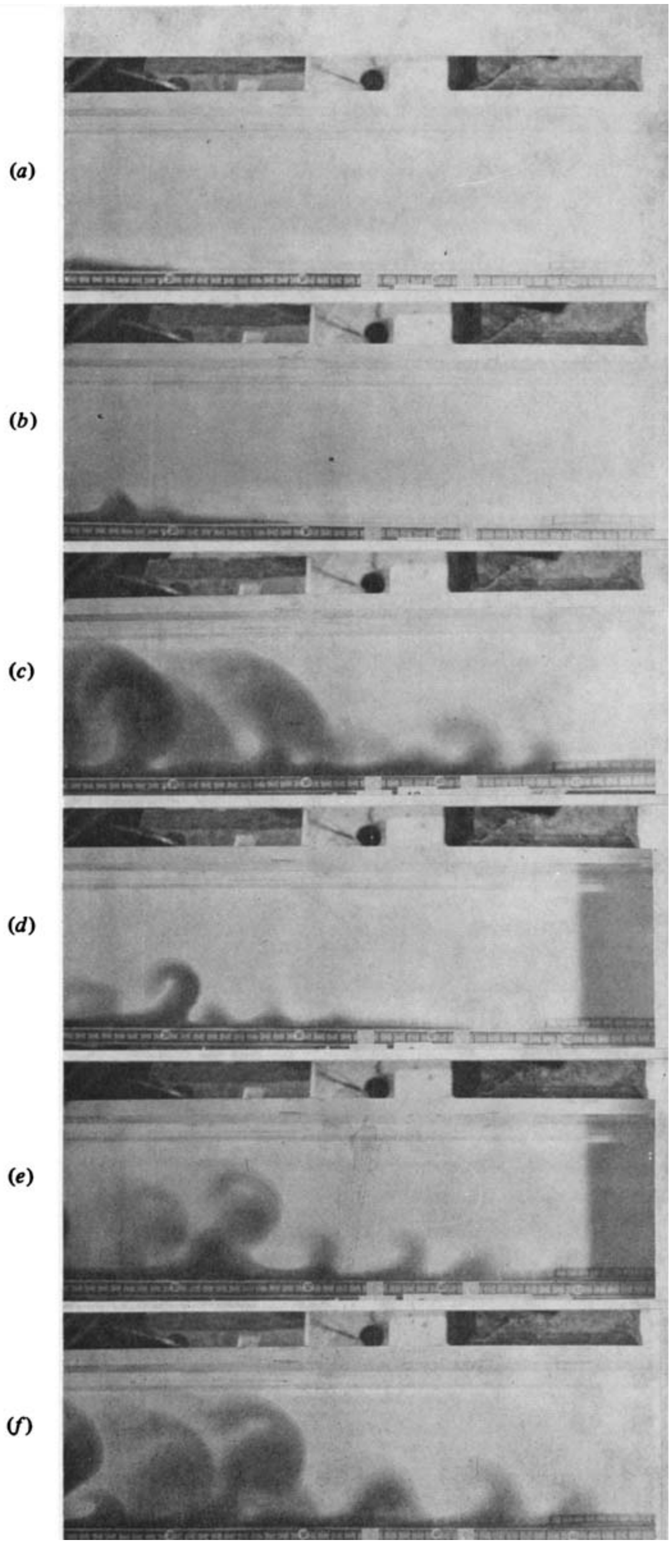
(a)
(b)
(c)
(d)
(e)
(f)